The HKU Scholars Hub   The University of Hong Kong   香港大學學術庫

Title	Ultraviolet Lasing Characteristics of ZnS Microbelt Lasers
Author(s)	Zhu, H; Su, SC; Yu, SF; Zhang, WF; Ling, FCC; Yang, HY
Citation	IEEE Journal of Selected Topics in Quantum Electronics, 2013, v. 19 n. 4, article no. 1501705
Issued Date	2013
URL	http://hdl.handle.net/10722/186163
Rights	IEEE Journal of Selected Topics in Quantum Electronics. Copyright © IEEE.

Ultraviolet Lasing Characteristics
of ZnS Microbelt Lasers

H. Zhu, S. C. Su, S. F. Yu, *Senior Member, IEEE*, W. F. Zhang, C. C. Ling, and H. Y. Yang

Abstract—Investigation on the room-temperature ultraviolet lasing characteristics of a single ZnS microbelt laser is presented. Lasing emission with peak wavelength at round 335 nm is observed from the hexagonal-wurtzite phase of ZnS microbelt under optical excitation. This is due to the Fabry–Perot resonance along the length of the microbelt. By studying the low-temperature and time-resolved photoluminescence, it is verified that the corresponding lasing characteristics are attributed to the excitonic optical gain process. Furthermore, the rectangular cross-sectional nanostructure of ZnS microbelt suppresses TM polarization for excitation power lower than ~1.4 times the threshold. Hence, ZnS microbelts can be a promising building block to realize ultraviolet semiconductor lasers with control of laser polarization.

Index Terms—Microcavities, semiconductor lasers, ZnS.

I. Introduction

Z nS, which has a wide bandgap (3.68 and 3.7 eV for cubic and hexagonal phase, respectively, at room temperature) and a large excitonic binding energy (40 meV) [1], is believed to be one of the promising ultraviolet (UV) optical materials. However, it is difficult to achieve room-temperature excitonic lasing emission from bulk or thin-film ZnS due to their high defect density [2]. Although there are extensive investigations on the optical characteristics of ZnS nanostructures, only few publications have reported lasing characteristics from nanostructured ZnS [3]–[6]. For example, Lee *et al*. had shown optical pumped amplified spontaneous emission from ZnS nanowires array [3]. Yang *et al*. had observed UV random lasing, which was arisen from the formation of closed-loop optical cavities, from the randomly distribution of ZnS nanosheets [6].

H. Zhu, S. F. Yu, and W. F. Zhang are with the Department of Applied Physics, The Hong Kong Polytechnic University, Kowloon, Hong Kong (e-mail: zhciomp@126.com; sfyu21@hotmail.com; wfzhang@msn.com).

S. C. Su is with the Institute of Optoelectronic Material and Technology, South China Normal University, Guangzhou 510631, China, and also with the Department of Physics, The University of Hong Kong, Hong Kong (e-mail: shichensu@yahoo.com.cn).

C. C. Ling is with the Department of Physics, The University of Hong Kong, Hong Kong (e-mail: ccling@hkucc.hku.hk).

H. Y. Yang is with the Pillar of Engineering Product Development, Singapore University of Technology and Design, 138682 Singapore (e-mail: yanghuiying@sutd.edu.sg).

Due to the high crystal quality, semiconductor nanostructures are considered to be a versatile building block for photonic applications [7], [8]. Lasing action has been observed from individual semiconductor microwires with hexagonal and triangular cross-sectional nanostructures [9], [10]. Nevertheless, the use of symmetric (i.e., relative to the axis of nanowires) cross-sectional nanostructures may have difficulty to suppress the one of the two polarizations so that they may not be the most appropriate choice for the photonic building block. In fact, there is no investigation on the use of rectangular nanostructures to suppress the emission polarization of semiconductor microcavities.

In this paper, we demonstrated low-threshold excitonic UV lasing from a single ZnS microbelt with rectangular cross-sectional nanostructure at room temperature. This is because of the 1) high excitonic gain of the hexagonal-wurtzite phase and low defect density of the ZnS microbelts as well as the 2) realization of coherent optical feedback along the length of ZnS microbelt. In addition, the rectangular nanostructure suppresses the generation of TM polarization for excitation power less than ~1.4 times the threshold. Thus, the use of ZnS microbelt is an alternative approach to fabricate UV photonic devices.

II. Fabrication and Characterization of ZnS Microbelts

High-crystal-quality ZnS microbelts were grown on a silicon substrate by vapor–liquid–solid method inside a horizontal tube furnace. The detail fabrication procedure can be found elsewhere [11]. The morphology of ZnS microbelts was characterized by field emission scanning electron microscopy (JEOL-JSM-7001 F). Transmission electron microscopy (TEM) images were obtained by a JEM-2010 TEM with accelerating voltage of 200 kV. Raman scattering spectra were investigated at room temperature in air by a HORIBA HR-800 with a laser emitted at 488 nm operating at a back scattering configuration. The time-resolved photoluminescence (TRPL) was measured by a Hamamatsu C5680-04 streak camera, and a tunable Ti:sapphire femtosecond-pulsed laser was an excitation source with the wavelength at 266 nm.

Fig. 1(a) displays the scanning electron microcopy (SEM) image of ZnS microbelts. As we can see, the as-growth samples have a belt-shaped morphology with length varying from 10 to 200 μm, an average width of ~2.5 μm, and an average thickness of ~200 nm. Fig. 1(b) shows a TEM image of a ZnS microbelt, which reveals that the microbelt has a sharp edge. Fig. 1(c) gives the high-resolution TEM image and the corresponding selected-area diffraction pattern. It is noted that the microbelts are a single-crystalline hexagonal phase ZnS structure and has a growth direction of <10-10>. Fig. 1(d) shows an
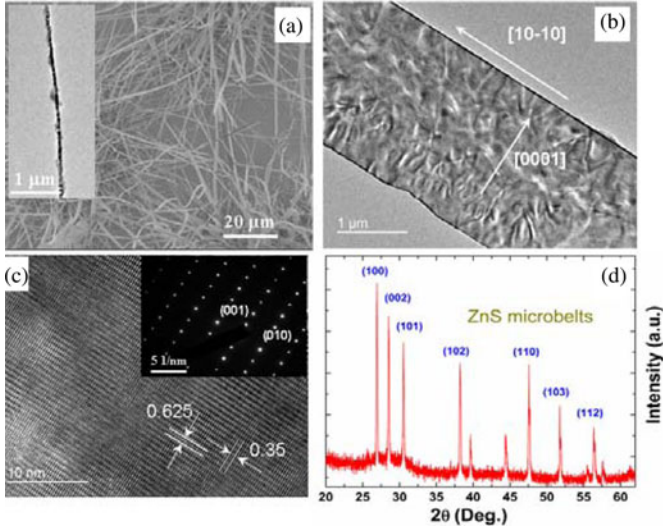
Fig. 1.   (a) SEM image of the randomly assembled ZnS microbelts. (b) TEM image and (c) high-resolution TEM image of a single ZnS microbelt; the inset is the corresponding diffraction pattern indicating <10-10> growth direction. (d) XRD diffraction pattern of the ZnS microbelts.
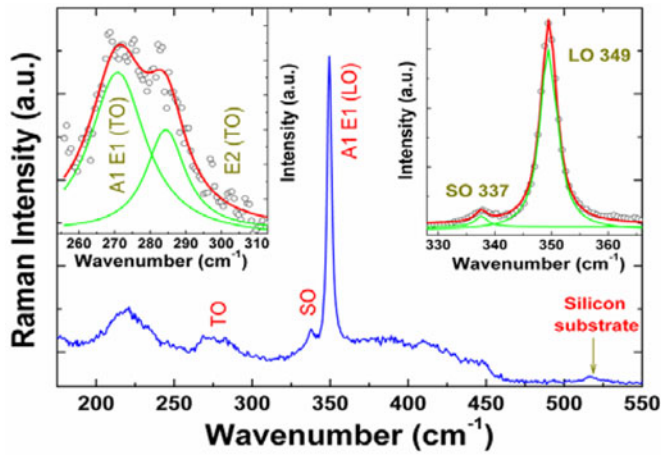

Fig. 2.   Microscopy Raman scattering spectrum from ZnS microbelts and fitting result. The two insets show the Lorentzian line shape fitting of the TO doublet ($270\,\mathrm{cm}^{-1}$, $285\,\mathrm{cm}^{-1}$) and LO ($349\,\mathrm{cm}^{-1}$) and SO ($337\,\mathrm{cm}^{-1}$) phonon modes.

X-ray diffraction (XRD) pattern of the ZnS microbelts. The XRD peaks reveal that the ZnS microbelts have a hexagonal wurtzite structure. This result is consistent with the TEM observation.

Raman scattering of ZnS microbelt is a local probe to access the crystalline quality, phase structure, and crystalline disorder of the components. Fig. 2 plots the Raman spectrum of the hexagonal phase ZnS microbelts. Strong first-order scattering from an unresolved doublet at $349\,\mathrm{cm}^{-1}$ is identified with A1 and E1 symmetry longitudinal optical (LO) modes. At lower frequency, a resolvable doublet is seen with peaks at 270 and $285\,\mathrm{cm}^{-1}$. These peaks are assigned to the A1/E1 and E2 transverse optical (TO) modes [12]. Furthermore, a peak at $337\,\mathrm{cm}^{-1}$, which is not seen from the bulk spectra, is due to surface optical (SO) phonon scattering. The essential characteristic of the Raman active surface optical phonon modes is that their peak
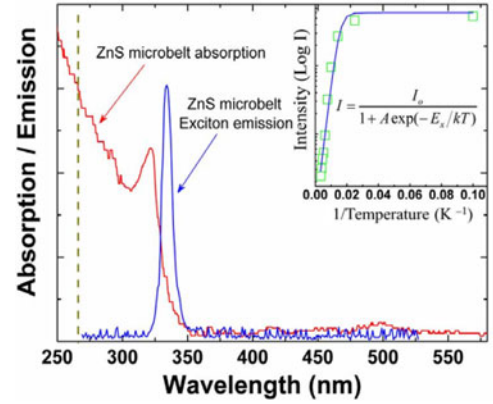

Fig. 3.   Absorption spectra and PL of the ZnS microbelts at room temperature. The inset plots the dependence of the exciton peak emission intensity at 335 nm on temperature. The solid line is the fitting of the experimental data.

intensity is sensitive to the surface roughness. The two insets of Fig. 2 show the results of a Lorentzian line shape fitting for the TO doublet and the nearby LO/SO mode. It is noted that the ratio of the fitting intensity between the LO and SO is 25:1 which indicates that the ZnS microbelts have smooth surfaces. Atomic force microscopy image (not shown here) also indicates that the ZnS microbelts have atom-scale surface flatness along the whole length. High crystal quality and smooth surface of ZnS microbelts are important for reducing the optical loss in the rectangular cross-section nanostructure, which is critical in achieving lasing oscillation.

III. Optical Behavior of ZnS Microbelts

Fig. 3 gives the absorption and photoluminescence (PL) spectrum of the ZnS microbelt at room temperature. An absorption peak located at 323 nm is clearly observed from the absorption spectrum. This peak is related to the free-exciton (FX) absorption in ZnS microbelts [13]. The room-temperature PL spectrum of the ZnS microbelts indicated that a dominant sharp emission peak is located at 335 nm and the deep-level emission is undetectable. These results indicate that the microbelts are free from defects and dislocations (i.e., nonradiative recombination centers that can lead to deep-level recombination transition). The emission mechanism of the ZnS microbelts can be investigated by the temperature-dependent PL measurement.

The inset of Fig. 3 plots the integrated intensity (from the peak of 335 nm) of the ZnS microbelts versus temperature. The emission intensity decreases monotonously with the increase of temperature. The variation trend of integrated intensity of the emission band $I(T)$ versus temperature T can be fitted by

$$I(T) = \frac{I_o}{1 + A\exp\left(-E_x/kT\right)} \quad (1)$$

where I_0 and A are constants to be fitted, k is the Boltzmann constant, and E_x is the activation energy. The best fitting of the data with (1) gives E_x to be $\sim$38 meV, which is identical to the FX binding energy of ZnS (40 meV) [1]. Therefore, the sharp emission peak located at 335 nm can be attributed to the FX emission of the ZnS microbelts [13].
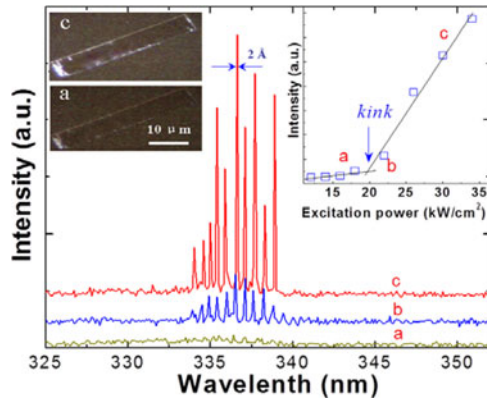
Fig. 4. Room-temperature lasing spectra of a single ZnS microbelt versus pump intensity. The insets show the light–light curve (top-right corner) and CCD images (top-left corner) of the single ZnS microbelt laser.
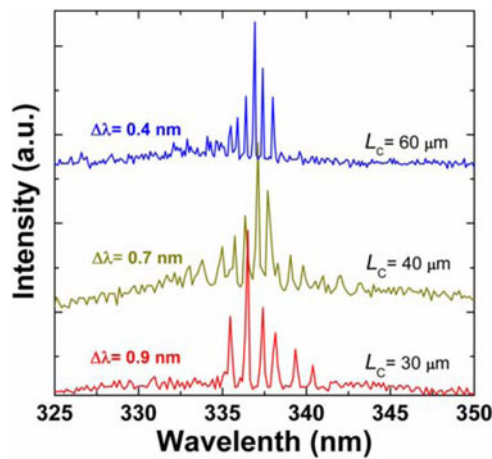

Fig. 6. Polar plot displays the integrated intensity of the lasing beam versus the angle of a linear analyzer at pump intensity of ~35 kW/cm^2. The ZnS microbelt is the same as shown in Fig. 4.

Fig. 5. Lasing spectra of the ZnS microbelt with different cavity lengths.

Fig. 7. TE and TM lasing spectra of the single ZnS microbelt at ~35 kW/cm^2. The inset shows the light–light curve of the TE and TM lasing modes.

Optical characteristics of an individual ZnS microbelt were studied by a quadruplet Q-switched Nd:YAG laser (at 266 nm) at pulsed operation (~6 ns, 10 Hz). A pump stripe of width less than 100 μm was collimated onto the surface of a single ZnS microbelt by a cylindrical lens. Emission from the edge of ZnS microbelt was then collected and analyzed by a monochromator. All the measurements were performed at room temperature. It can be seen from Fig. 4 that the single ZnS microbelt exhibits spontaneous emission at low excitation power (~15 kW/cm^2). The length of the ZnS microbelt is about 40 μm. When the pump power increases to a threshold, P_{th}, (~20 kW/cm^2), sharp peaks with linewidth < 2 Å emerge from the broad emission spectrum. It is noted that the sharp peaks are equally spacing across the emission spectrum above the threshold. The light output versus optical excitation power density curve of the ZnS microbelt is also inserted onto the top-right corner of Fig. 4. Two photos inserted onto the top-left corner of Fig. 4 show emission characteristics of the ZnS microbelt under the excitation below and above the threshold. Strong emission intensity is observed from the edges of the ZnS microbelt under excitation above the threshold. Hence, it is verified that the ZnS microbelt exhibits lasing oscillation.
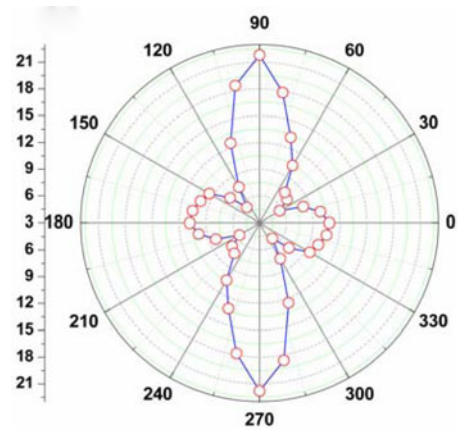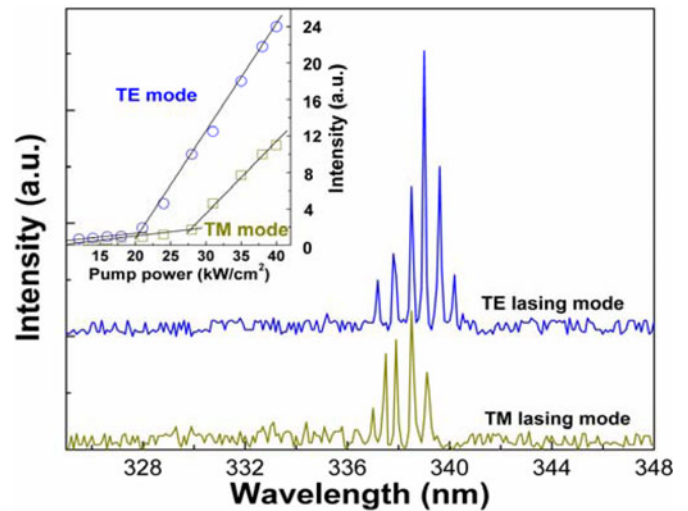
Fig. 5 displays the lasing spectra of single ZnS microbelts versus different length with the pump power kept at ~25 kW/cm^2. The sharp peaks have equally spacing $\Delta\lambda$ throughout the emission spectrum and $\Delta\lambda$ varies from 0.15 to 0.5 nm for the reduction of length of the ZnS microbelts. The uniform spacing of sharp peaks is attributed to the longitudinal Fabry–Perot resonance arisen from the optical feedback from the two facets of the ZnS microbelt. $\Delta\lambda$ of a Fabry–Perot cavity can be deduced from $\Delta\lambda \approx \lambda_0^2/2n_{\text{eff}}L_c$, where n_{eff} is the effective optical mode refractive index of the ZnS at wavelength λ_0, and L_c is the longitudinal cavity length of the microbelts [14]. If λ_0 is assumed to be ~337 nm and using the results of $\Delta\lambda$ given in Fig. 5 for some value of L_c, the average value of n_{eff} can be found to be ~2.30. This value of n_{eff} is closed to our theoretical studies of ZnS microbelts with refractive index of bulk ZnS set to ~2.40 [15].

Figs. 6 and 7 study the polarization characteristics of the ZnS microbelt excited at ~1.8 times of the threshold. The ZnS microbelt used in Figs. 6 and 7 is the same as that used in Fig. 4. The polar plot in Fig. 6 displays the edge emission intensity of
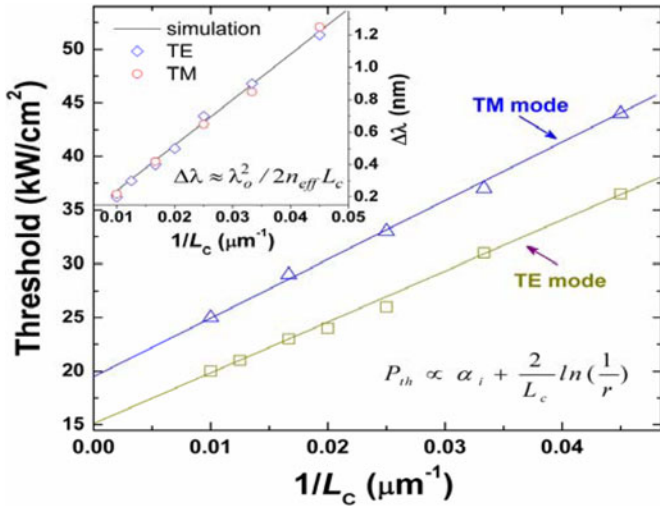
Fig. 8.   Plots of measured and calculated values of P_{th} and $\Delta\lambda$ versus L_c for both TE and TM lasing modes of a single ZnS microbelt laser.
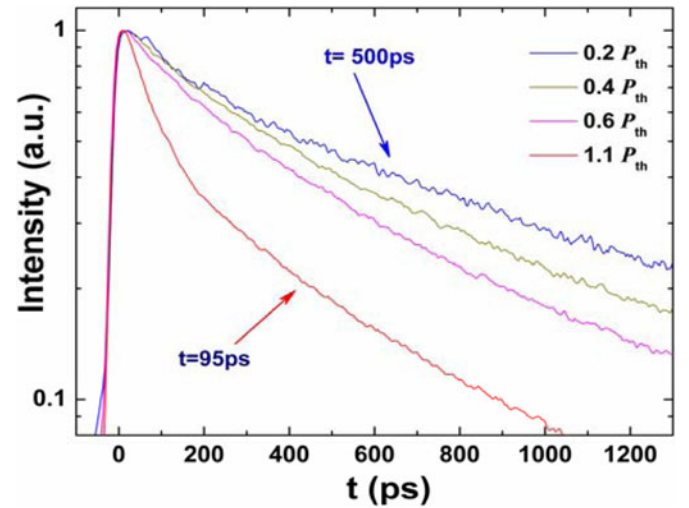

Fig. 9.   Evolution from spontaneous emission to lasing with increasing pump density by using the TRPL technique. The single-exponential decay time constant at low pump density varies between 500 and 300 ps. However, the decay time collapses to 95 ps above the threshold.

a ZnS microbelt through a linear polarizer versus the rotation angle θ. $\theta = 0°$ (90°) represents the electric field polarized along the width (thickness) of the ZnS microbelt. The pump power of the ZnS microbelt was kept at $\sim$35 kW/cm^2. The plot indicates that the ZnS microbelt can support two orthogonally polarized fields. The electric field polarized along the width of the ZnS microbelt (i.e., TE modes) is dominant by the emission spectra and that along the thickness of the ZnS microbelt (i.e., TM modes) is suppressed by the rectangular cross-sectional stripe-waveguide structure.

Fig. 7 plots the emission spectra of TE and TM modes at pump power of $\sim$35 kW/cm^2. It is noted that TE modes have higher emission intensity than that of TM modes because the threshold of TE modes is $\sim$10 kW/cm^2 lower than that of the TM modes. Therefore, TM modes will be suppressed in the emission spectra of ZnS microbelt if the pump intensity is less than $P_{\text{th}} \sim$30 kW/cm^2.

Threshold P_{th} and mode spacing $\Delta\lambda$ for both TE and TM modes of the ZnS microbelts versus L_c are displayed in Fig. 8. The total internal optical loss and reflectivity ratio between TE and TM modes inside the ZnS microbelt can be deduced from the following equation:

$$P_{\text{th}} \propto \alpha_i + \frac{2}{L_c}\ln\left(\frac{1}{r}\right) \qquad (2)$$

where α_i is the total internal optical losses, r is the field reflectivity of the ZnS microbelt facets by fitting (2) with the measured values of P_{th} and L_c. It is noted that $\ln(1/r_{TE})/\ln(1/r_{TM})$ $\sim$0.967 so that $r_{\text{TE}} > r_{\text{TM}}$ for the ZnS microbelts is expected. From the y-intercept of the lines in Fig. 8, the ratio of α_i between TM and TE modes $\alpha_{i\text{TM}}/\alpha_{i\text{TE}}$ can be deduced to be (19/15) $\sim$1.267. This indicates that the waveguide losses of the ZnS microbelts of TM modes are larger than that of the TE modes. Hence, TE modes are dominant in the lasing spectra due to the corresponding large (low) value of r_{TE} ($\alpha_{i\text{TE}}$). The inset of Fig. 8 shows plots $\Delta\lambda$ versus $1/L_c$. It is observed that $\Delta\lambda$ of both TE and TM modes is proportional to $1/L_c$. The solid line

is the calculated value of $\Delta\lambda$ versus L_c according to (1). The value of n_{eff} for TE and TM modes is found to be $\sim$2.30.

The optical gain mechanism of the ZnS microbelts was investigated by using the TRPL technique. The plot of time-dependence integrated intensity, which was originated from exciton emission peak at 335 nm, is illustrated in Fig. 9. At pump power equal to $\sim$0.02 $\times P_{\text{th}}$, the emission follows a multiexponential decay with lifetime of $\sim$500 ps. At higher pump density, the emission lifetime is further reduced to a shorter decay lifetime. When the excitation density exceeds the threshold, the emission decay lifetime collapses to 95 ps as shown in the PL trace. The fast relaxation behavior is essentially identical to that of the optical pump ZnS microbelts lasing process. This can been considered as evidence of many particle effects in the high exciton density region (exciton–exciton interactions, exciton–carrier interactions, and exciton–phonon interactions) for the optical gain to be build up inside nanostructures [16], [17].

IV. CONCLUSION

A single ZnS microbelt laser with rectangular cross-sectional nanostructure was realized to support low-threshold excitonic UV lasing at room temperature. The excitonic optical gain process, which is verified by the low-temperature PL and TRPL, is attributed to the high excitonic gain of ZnS microbelts. The excitation of lasing modes is arisen from the Fabry–Perot resonance between the two facets of the ZnS microbelts. Due to the geometry of rectangular nanostructures, lasing modes supported inside the ZnS microbelt are TE dominant at excitation power less than $\sim$1.4 times the threshold. The ratio of α_i between TM and TE modes is also found to be $\sim$1.267. Hence, high optical quality of ZnS microbelts can be a promising building block to realize UV semiconductor lasers.

REFERENCES

[1] A.P. Goswami, "Dielectric and optical properties of ZnS films," *Thin Solid Films*, vol. 16, pp. 175–185, 1973.

[2] T. K. Tran, W. Park, W. Tong, M. M. Kyi, B. K. Wagner, and C. J. Summers, "Photoluminescence properties of ZnS epilayers," *J. Appl. Phys.*, vol. 81, pp. 2803–2809, 1997.

[3] Y. Jiang, W.J. Zhang, J.S. Jie, X.M. Meng, J.A. Zapien, and S.T. Lee, "Homoepitaxial growth and lasing properties of ZnS nanowire and nanoribbon arrays," *Adv. Mater.*, vol. 18, pp. 1527–1532, 2006.

[4] J.X. Ding, J.A. Zapien, W.W. Chen, Y. Lifshitz, S.T. Lee, and X.M. Meng, "Lasing in ZnS nanowires grown on anodic aluminum oxide templates," *Appl. Phys. Lett.*, vol. 85, pp. 2361–2363, 2004.

[5] X.T. Zhang, Y.C. Liu, L.G. Zhang, J.Y. Zhang, Y.M. Lu, D.Z. Shen, W. Xu, G.Z. Zhong, X.W. Fan, and X.G. Kong, "Structure and optically pumped lasing from nanocrystalline ZnO thin films prepared by thermal oxidation of ZnS thin films," *J. Appl. Phys.*, vol. 92, pp. 3293–3298, 2002.

[6] H.Y. Yang, S.F. Yu, J. Yan, and L. D. Zhang, "Random lasing action from randomly assembled ZnS nanosheets," *Nanoscale Res. Lett.*, vol. 5, pp. 809–812, 2010.

[7] C. Ma, D. Moore, J. Li, and Z.L. Wang, "Microbelts, nanocombs, and nanowindmills of wurtzite ZnS," *Adv. Mater.*, vol. 15, pp. 228–231, 2003.

[8] X.S. Fang, T.Y. Zhai, U.K. Gautam, L. Li, L. M. Wu, Y. Bando, and D. Golberg, "ZnS nanostructures: From synthesis to applications," *Progr. Mater. Sci.*, vol. 56, pp. 175–287, 2011.

[9] C. Czekalla, C. Sturm, R. Schmidt-Grund, B. Cao, M. Lorenz, and M. Grundmann, "Whispering gallery mode lasing in zinc oxide microwires," *Appl. Phys. Lett.*, vol. 92, pp. 241102-1–241102-3, 2008.

[10] C. Czekalla, J. Lenzner, A. Rahm, T. Nobis, and M. Grundmann, "A zinc oxide microwire laser," *Superlattices Microstruct.*, vol. 41, no. 5–6, pp. 347–351, 2007.

[11] Y. Wang, L.D. Zhang, C.H. Liang, G.Z. Wang, and X.S. Peng, "Catalytic growth and photoluminescence properties of semiconductor single-crystal ZnS nanowires," *Chem. Phys. Lett.*, vol. 357, pp. 314–318, 2002.

[12] Q. H. Xiong, J. G. Wang, O. Reese, L. C. Lew Yan Voon, and P. C. Eklund, "Raman scattering from surface phonons in rectangular cross-sectional w-ZnS nanowires," in *Proc. Nano Lett.*, 2004, vol. 4, pp. 1991–1996.

[13] S. Nakamura, T. Sakashita, K. Yoshimura, Y. Yamada, and T. Taguchi, "Temperature dependence of free-exciton luminescence from high-quality ZnS epitaxial layers," *Jpn. J. Appl. Phys.*, vol. 36, pp. L491–L493, 1997.

[14] L. A. Coldren and S. W. Corzine, *Diode Lasers and Photonic Integrated Circuits*.   New York, NY, USA: Wiley, 1995.

[15] I. C. Ndukwe, "Solution growth, characterization and applications of zinc sulphide thin films," *Solar Energy Mater. Solar Cells*, vol. 40, pp. 123–131, 1996.

[16] V.I. Klimov, C.J. Schwarz, D.W. McBranch, C.A. Leatherdale, and M.G. Bawendi, "Ultrafast dynamics of inter- and intraband transitions in semiconductor nanocrystals: Implications for quantum-dot lasers," *Phys. Rev. B*, vol. 60, pp. R2177–R2180, 1999.

[17] C. Klingshirn, *Semiconductor Optics*, 2nd ed.   New York, NY, USA: Springer, 2005.

S. C. Su received the Ph.D. degree from the Changchun Institute of Optics, Fine Mechanics and Physics, Chinese Academy of Sciences, Changchun, China.

He is currently a Research Fellow in the Department of Physics, The University of Hong Kong, Hong Kong. He is also with the Institute of Optoelectronic Material and Technology, South China Normal University, Guangzhou, China.

S. F. Yu (M'03–SM'03) received the B.Eng. degree from the University College London, London, U.K., in 1990, and the Ph.D. degree in optoelectronics engineering from Cambridge University, Cambridge, U.K., in 1993.

He is currently a Professor in the Department of Applied Physics, The Hong Kong Polytechnic University, Kowloon, Hong Kong. He has authored or coauthored more than 300 referred journal and conference papers, book chapters, and one book entitled *Analysis and design of VCSELs* (Wiley, 2003). His main research interests include the fundamental study, design, and optimization of semiconductor lasers including distributed feedback lasers and vertical-cavity surface-emitting lasers.

W. F. Zhang received the B.Sc. and M.Sc. degrees in chemistry from Shanghai University, Shanghai, China. He is currently working toward the Ph.D. degree at The Hong Kong Polytechnic University, Kowloon, Hong Kong.

C. C. Ling received the B.Sc., M.Phil., and Ph.D. degrees from The University of Hong Kong, Hong Kong.

He is currently an Associate Professor in the Department of Physics, The University of Hong Kong.

H. Y. Yang received the Ph.D. degree from Nanyang Technological University (NTU), Singapore, in 2007.

She is currently an Assistant Professor at the Singapore University of Technology and Design, Singapore. Her research expertise lies in nanomaterials and devices. From July 2006 to June 2008, she was a Singapore Millennium Foundation Postdoctoral Fellow at NTU, where from July 2008 to October 2010, she was a Lee Kuan Yew Postdoctoral Fellow. She has published more than 60 peer-reviewed articles in major scientific journals, with more than 550 citations and an H-index of 13.

Dr. Yang received the prestigious Lee Kuan Yew Fellowship in 2008, the Singapore Millennium Foundation Fellowship in 2006, the L'Oreal Singapore for Women in Science National Fellowship in 2010, the Chinese Government Award for Outstanding Self-Financed Students Abroad in 2005, the Second Prize in Material Research Society Science-as-Art Competition in 2008, and the First Prize in NTU Nanoscience-as-Art Competition in 2005.

H. Zhu received the B.E. degree from the School of Optoelectronic Engineering, Changchun University of Sciences and Technology, Changchun, China, in 2006, and the Ph.D. degree from the Changchun Institute of Optics, Fine Mechanics and Physics, Chinese Academy of Sciences, Changchun, in 2010.

He is currently a Research Fellow in the Department of Applied Physics, The Hong Kong Polytechnic University, Kowloon, Hong Kong.